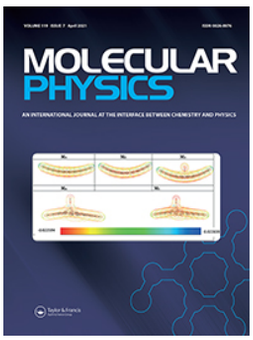

Taylor & Francis
Taylor & Francis Group

Molecular Physics

An International Journal at the Interface Between Chemistry and Physics

ISSN: (Print) (Online) Journal homepage: https://www.tandfonline.com/loi/tmph20

Theoretical approaches for doubly-excited Rydberg states in quasi-two-electron systems: two-electron dynamics far away from the nucleus

M. Génévriez

To cite this article: M. Génévriez (2021) Theoretical approaches for doubly-excited Rydberg states in quasi-two-electron systems: two-electron dynamics far away from the nucleus, Molecular Physics, 119:7, e1861353, DOI: 10.1080/00268976.2020.1861353

To link to this article: https://doi.org/10.1080/00268976.2020.1861353

Published online: 18 Dec 2020.

MOLECULAR PHYSICS
2021, VOL. 119, NO. 7, e1861353 (16 pages)
https://doi.org/10.1080/00268976.2020.1861353

Taylor & Francis
Taylor & Francis Group

NEW VIEW

Theoretical approaches for doubly-excited Rydberg states in quasi-two-electron systems: two-electron dynamics far away from the nucleus

M. Génévriez

Laboratory of Physical Chemistry, ETH Zurich, Zurich, Switzerland

ABSTRACT

We report on recent progress regarding the theoretical treatment of doubly-excited Rydberg states of atoms with two valence electrons. Building upon state-of-the-art techniques, we demonstrate that an approach based on configuration interaction with exterior complex scaling (CI-ECS) is capable of describing high Rydberg states ($n \sim 100$) and does not rely on the assumptions of R-matrix multichannel quantum-defect theory. We show that CI-ECS allows the simultaneous, accurate treatment of a range of doubly-excited Rydberg states broader than previously possible. The implementation of the method with numerical basis functions is explained in detail. As an example, CI-ECS calculations of the doubly-excited states of Mg and Sr are presented, and excellent agreement is found with available experimental data. The CI-ECS method opens new perspectives for studying collective two-electron dynamics in doubly-excited Rydberg states of alkaline-earth metal atoms, and is also of interest for the field of Rydberg-based quantum simulation.

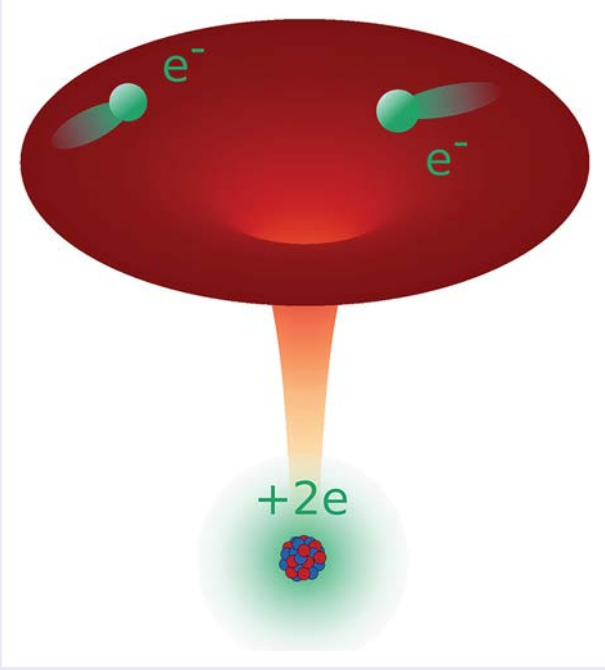

ARTICLE HISTORY
Received 7 September 2020
Accepted 27 November 2020

KEYWORDS
Rydberg state; autoionisation; doubly-excited state; exterior complex scaling; configuration interaction;

1. Introduction

The quantum-mechanical motion of two electrons and a nucleus, coupled by Coulomb interactions, stands as one of the fundamental examples of the microscopic three-body problem. Not only did the helium atom stimulate the development of modern quantum mechanics, but two-electron atoms and ions have since become ideal systems to study basic aspects of electron correlations and dynamics [1], and often act as stepping stones to tackle many-body problems. A large amount of experimental

CONTACT M. Génévriez matthieu.genevriez@phys.chem.ethz.ch Laboratory of Physical Chemistry, ETH Zurich, Zurich CH-8093, Switzerland

This article has been corrected with minor changes. These changes do not impact the academic content of the article.

and theoretical methods have been and are still being developed to study the correlated motion of two electrons in three-body systems with an exquisite amount of detail [2–5]. This 'New Views' article discusses theoretical advances in this domain for atomic systems possessing only two valence electrons. These electrons can be considered as independent from the residual closed-shell ionic core, and such atoms thus form *quasi-two-electron* systems. They are for example the alkaline-earth metals (Be, Mg, Ca, Sr, Ba) or Yb. Whereas, in the helium atom, correlated electronic motion in doubly-excited states has been investigated in numerous theoretical works (see Tanner *et al.* [2] for a review), this subject remains largely unexplored in quasi-two-electron systems. In contrast, experimental data on He is limited to excitation of relatively low-lying doubly-excited states with low orbital angular momentum ($L = 0-2$) [6–13], whereas experiments on a much broader range of doubly-excited states were carried out in alkaline-earth metal atoms [14–22]. The theoretical developments reported below aim at reaching a better understanding of two-electron dynamics in high-lying doubly-excited states of quasi-two-electron systems through first principles calculations. These calculations also aim at disentangling the very dense and complex spectra recorded in pioneering experiments [16,18,19,21,22] and assess the range of validity of the qualitative models developed to describe them. Finally, the accurate theoretical description of core-excited Rydberg states is of interest for quantum optics and quantum simulation because manipulating Rydberg atoms by optically driving a transition in the residual ionic core, thus producing doubly-excited states, opens interesting perspective in these domains and is a goal that is actively pursued [23–29].

Rydberg states are associated with electrons promoted to atomic orbitals that are much larger in size than the residual ion 'core'. Rydberg electrons are labelled by their principal quantum number n, orbital-angular-momentum quantum number l and total-angular-momentum quantum number j. In the following, we distinguish three different types of Rydberg states: (i) singly-excited Rydberg states, in which one electron is in a Rydberg orbital and the ion core is in its electronic ground state; (ii) core-excited Rydberg states, in which one electron is in a Rydberg orbital and the ion core is in a low-lying excited electronic state; (iii) doubly-excited Rydberg states, where two electrons are in Rydberg orbitals. These three types of Rydberg states possess distinctive physical properties that are detailed below for the case of quasi-two-electron atoms.

In singly-excited Rydberg states, only one electron of the quasi-two-electron atom is excited. In this case, the two electrons occupy largely different regions of phase space. They can be considered as independent and are consequently well described by a single electronic configuration (*e.g.* [Ne]3*s*20*p* in Mg). The energies of singly-excited Rydberg states follow in most cases the Rydberg formula

$$E_n = E_I - \frac{Ry}{(n-\delta_l)^2}, \tag{1}$$

where Ry is the Rydberg constant and δ_l is the quantum defect, which depends on the orbital angular momentum l of the Rydberg electron. The development of multi-channel quantum-defect theory (MQDT) [30–33] has offered a unified picture of the physical origin of quantum defects and of the local deviations from the Rydberg formula observed, for example, in Sr, Ba or Yb (see, *e.g.* Refs. [34–36], respectively). Quantum defects are understood as arising from the elastic scattering of the Rydberg electron off the core, which results in the appearance of an additional phase shift in the Rydberg-electron wave function. Inelastic scattering couples different Rydberg series together and this interaction induces local displacements of the energy levels. In MQDT, a large number of Rydberg states and series can be described by only a small number of scattering parameters, that can either be fitted to reproduce experimental data or calculated *ab inito* [31,33,37–39].

When both electrons are excited, the situation is more complicated. This is illustrated in Figure 1 by a schematic view of the energy-level structure of the doubly-excited states of Mg. The energy levels were calculated within the independent-electron approximation, *i.e.* neglecting all electron-electron correlations except the screening of the doubly-charged ionic core by the inner electron. Rydberg series can be observed that converge to each individual level of the ionic core and, because the density of core levels increases with the degree of excitation, the density of doubly-excited states states also increases very rapidly. States belonging to these series have energies above the first ionisation threshold and can thus decay by autoionisation [40], a process in which an electron is spontaneously emitted, leaving the ionic core in a state of lower energy. Their theoretical treatment must thus (i) include continuum states and (ii) deal with the increasing density of perturbations.

Core-excited Rydberg states are depicted in red in Figure 1 and correspond to the situation where one of the two electrons is in a Rydberg state while the other is excited to a comparatively low-lying state of the ionic core ($n_2 \gg n_1$). The increase in the density of states causes more frequent deviations from the Rydberg formula compared to singly-excited Rydberg states. Because of the *asymmetric* excitation of the two electrons, these typically reside at very different distances

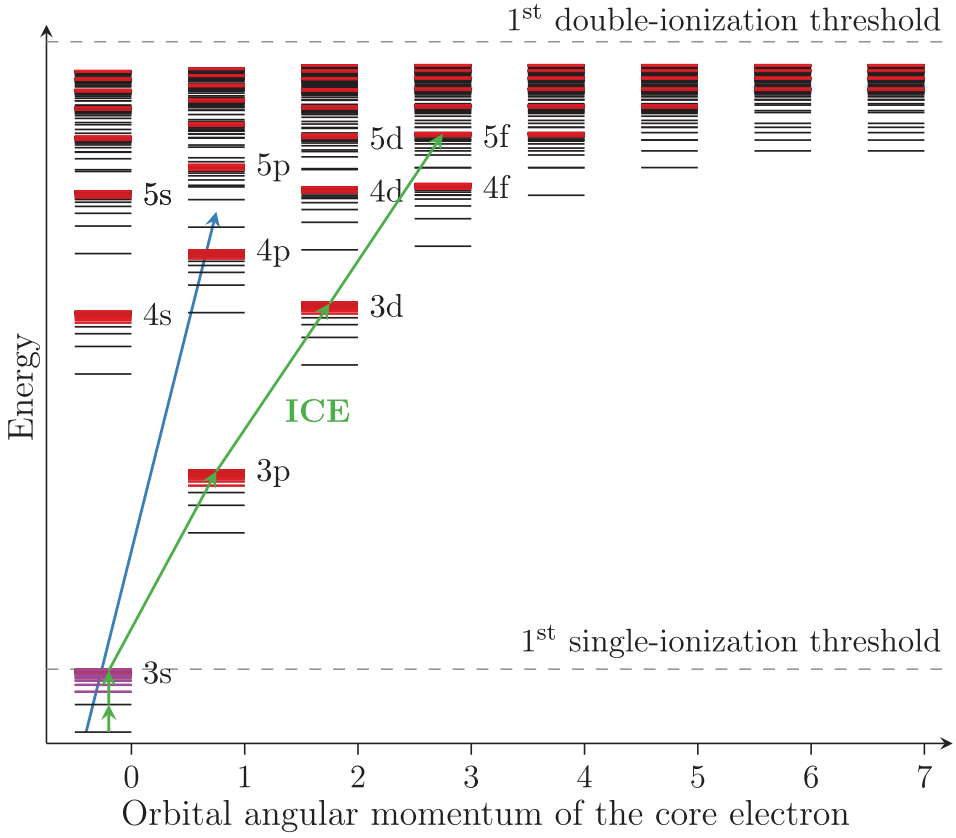

Figure 1. Schematic representation of the energy-level structure of singly-excited states ([Ne]3sn_2l_2) and doubly-excited states ([Ne]$n_1l_1n_2l_2$) of Mg. For simplicity, only one Rydberg series per threshold is represented. The purple lines designate singly-excited Rydberg states. The red lines show core-excited Rydberg states ($n_2 \gg n_1$), which lie just below the ion thresholds. They are too closely-spaced to be resolved on the scale of the figure. The lowest-lying thresholds are labelled by the corresponding electronic configurations of the singly-charged ion, Mg^+([Ne]nl). The blue and green arrows represents different excitation schemes from atoms in their ground electronic state to doubly-excited states (see text). The blue arrow depicts single-photon absorption and the green arrows give an example of multiphoton isolated-core excitation (ICE).

from the nucleus ($\langle r_2 \rangle \gg \langle r_1 \rangle$) and occupy largely different phase-space regions. In many cases, perturbations arising from dynamical electron-electron correlations are small and the independent-electron picture represents a reasonable approximation. For example, many core-excited Rydberg states of the alkaline-earth metals or the rare gases are well described by a single electronic configuration [33,41]. An independent-electron model, the isolated-core-excitation (ICE) approximation [14], is also successful in describing many spectra associated with the excitation of alkaline-earth atoms from singly-excited Rydberg states to core-excited Rydberg states [14,15,17,33,42,43].

As the degree of excitation of the core electron increases, the strength of the Coulomb attraction of the nucleus decreases and the strength of the bielectronic repulsion increases. States in this region correspond to doubly-excited Rydberg states ($n_2 \sim n_1$). The regions of phase space occupied by the two electrons start overlapping and the independent-electron approximation breaks down. In Figure 1, this situation corresponds to the region where the differences between adjacent energy levels of the Rydberg electron are comparable to those of the core electron. Perturbations between Rydberg series converging to different thresholds are ubiquitous and the Rydberg formula is not applicable. Doubly-excited Rydberg states in this range cannot be described effectively by a single electronic configuration and the motion of the two electrons is strongly correlated. Although some experiments were carried out in alkaline-earth metal atoms in this region [16,18,19,21,22,44], their theoretical interpretation is far from complete.

In the literature, the study of doubly-excited states is divided between 'genuine' two-electron systems (H^-, He) and quasi-two-electron systems such as alkaline-earth metal atoms. The former are attractive theoretically because of their simplicity and fundamental nature but, on the other hand, experimental studies are considerably hampered by the large excitation energies of such systems which prevents the application of high-resolution

laser excitation. The latter are attractive experimentally because of their considerably lower excitation energies that permit flexible excitation schemes with visible and UV lasers, whereas theoretical investigations are complicated by the presence of a closed-shell ionic core, which in particular lifts the l-degeneracy of the energy levels of the singly-charged ionic core, and the relatively strong spin-orbit interaction.

A large body of theoretical work has been devoted to the description of doubly-excited states of helium using classical, semiclassical and quantum-mechanical methods [2]. Herrick and co-workers established the existence of an approximate but complete set of quantum numbers describing the collective motion of the two electrons (for a review, see Herrick [45]). However, the assignment of these quantum numbers to particular resonances becomes increasingly difficult for higher excitation because of the increasing amount of perturbations between Rydberg states belonging to series converging to different thresholds [46]. A large portion of the helium phase space is chaotic [47] and periodic-orbit semiclassical chaos theory [48] proved useful in analysing regions of the He spectrum where many resonances overlap [49,50]. Perhaps surprisingly, some regions of the doubly-excited He phase space are classically stable [51] and correspond to configurations where both electrons are dynamically localised on the *same* side of the nucleus. Their quantum analogue, the so-called 'frozen planet states' or *Zee* configurations, are also predicted to exist [52,53] but are yet to be observed experimentally. Most theoretical developments in the field have relied on the comparison of a large number of observables (*e.g.* energies, widths, relative angles or electronic densities) calculated using classical, semiclassical and quantum-mechanical models with the results of large-scale 'exact' calculations [2].

Most experimental studies of doubly-excited Rydberg states of helium rely on the observation of resonances in the ionisation cross section of ground state atoms (blue arrow in Figure 1). Following the pioneering work of Madden and Coddling [54], a number of synchrotron measurements allowed the observation of doubly-excited Rydberg states with total orbital angular momentum $L = 1$ lying below the $He^+(n = 15)$ threshold [6–10,13]. A number of low-lying doubly-excited states were also observed in electron-impact-ionisation studies (see Ref. [12] for a recent example). Core-excited Rydberg states with a principal quantum number of the Rydberg electron larger than ∼25 and doubly-excited Rydberg states lying above the $He^+(n = 15)$ threshold have not been observed, most likely because of the limited energy resolution of experiments using synchrotron radiation or electron beams and because the excitation efficiency decreases with the degree of excitation [9,55,56].

In parallel, numerous works have been dedicated to the characterisation of core-excited Rydberg states of alkaline-earth metal atoms, and were instrumental in the understanding of autionisation processes and in the development of MQDT [33]. A much broader range of core-excited and doubly-excited Rydberg states have been accessed experimentally compared to helium, because of the possibility to use the ICE technique with conventional laser systems [14]. In the ICE technique, depicted by the green arrows in Figure 1, the atom is first prepared in a singly-excited Rydberg state by single- or multi-photon excitation and the core electron is subsequently excited by further photoabsorption. The multiphoton approach, combined with the fact that each excitation step corresponds to a very efficient one-electron resonant excitation, gives considerable flexibility in the preparation of doubly-excited Rydberg states. Combined with the Stark-switching technique [57], ICE allows the preparation of doubly-excited states with a large range of orbital angular momenta of the Rydberg electron [14,58]. Core-excited circular Rydberg states, in which the Rydberg electron possesses maximal angular-momentum and magnetic quantum numbers ($l_2 = n_2 - 1, m_{l_2} = l_2$), have also been prepared with ICE [29,59]. Multiphoton excitation of the core electron permits the study of multiple core-excited Rydberg series [60–64] and allows the exploration of core-excitation regimes where electron-electron correlations have a noticeable influence on ICE spectra [16,18,19,21,22,65,66].

Theoretical treatments of two-electron dynamics in high-lying doubly-excited Rydberg states of alkaline-earth metal atoms are limited to simple electrostatic models that provide a qualitative understanding of multiphoton ICE spectra [16,18,19,22,62,66], and to an extension of the R-matrix MQDT method [67]. Predictions of, *e.g.* two-electron charge densities, were proposed based on an electrostatic model which treats the polarisation of the inner-electron wave function by the electric field generated by the Rydberg electron as a Stark effect [16,19]. Comprehensive calculations of two-electron resonances and wave functions from first principles, as is routinely achieved in studies in helium, have not been carried out to date. The present 'New Views' article describes progress in this direction. Such calculations would: (i) provide the accurate energies and autoionisation widths of a broad range of singly-excited, core-excited and doubly-excited Rydberg states; (ii) permit an independent assessment of the models based on the polarisation of the inner electron by the Stark effect; (iii) enable the systematic exploration of a broad range of double-excitation regimes while providing access to

observables relevant to the study of correlated electron dynamics such as two-electron charge densities and interelectronic angles. Furthermore, point (i) is of interest for the development of quantum simulators based on alkaline-earth metals since it would allow, for example, to screen a large number of core-excited Rydberg states and identify those exhibiting the most promising properties for the experiments. Point (iii) is crucial in assessing whether frozen-planet states similar to those predicted in helium (see discussion above) also exist in quasi-two-electron systems and whether their observation, which remains elusive, is possible in alkaline-earth metals.

The article is structured as follows: in Section 2, existing theoretical methods for studying doubly-excited Rydberg states are reviewed, and a possible route for investigating them in alkaline-earth metals is described, which is based on large-scale configuration-interaction calculations with exterior complex scaling (CI-ECS); in Section 3, the validity and accuracy of the CI-ECS method are assessed by studying core-excited Rydberg states of Mg, and the method is then used to calculate, from first principles, photoexcitation spectra to doubly-excited states of Sr for which the independent-electron approximation is clearly violated [22].

2. Theoretical approaches for doubly-excited Rydberg states

Quasi-two-electron systems such as alkaline-earth metal atoms are well described by the following two-active-electron Hamiltonian [33],

$$\hat{H}(\boldsymbol{r_1},\boldsymbol{r_2}) = -\frac{1}{2}\boldsymbol{\nabla}_1^2 - \frac{1}{2}\boldsymbol{\nabla}_2^2 + V_{l_1}(r_1) + V_{l_2}(r_2) + V^{\mathrm{SO}}_{s_1 l_1 j_1}(r_1) + V^{\mathrm{SO}}_{s_2 l_2 j_2}(r_2) + \frac{1}{r_{12}} + V^{(2)}_{\mathrm{pol}}(\boldsymbol{r_1},\boldsymbol{r_2}), \tag{2}$$

where $\boldsymbol{r_1}$ and $\boldsymbol{r_2}$ are the position vectors associated with the two electrons, described by the independent-electron orbital-, spin- and total-angular-momentum quantum numbers l_1, s_1, j_1 and l_2, s_2, j_2, respectively. $r_{12} = |\boldsymbol{r_1} - \boldsymbol{r_2}|$ is the distance between the two electrons. The bielectronic Coulomb repulsion $(1/r_{12})$ and bielectronic polarisation $(V^{(2)}_{\mathrm{pol}})$ terms are responsible for electron correlations and configuration mixing. Atomic units are used in this section unless stated otherwise. Finite-nuclear-mass effects are neglected for simplicity. The l-dependent model potential $V_{l_i}(r)$ $(i = 1, 2)$ accounts for the interaction of the valence electrons with the closed-shell doubly-charged ionic core, either in an empirical [33] or semi-empirical [68] manner. It is different for each alkaline-earth element. In the work presented below, the potential form reported in Ref. [33],

$$V_l(r) = -\frac{1}{r}\left[2 + (Z-2)\mathrm{e}^{-\alpha_1^l r} + \alpha_2^l \mathrm{e}^{-\alpha_3^l r}\right] - \frac{\alpha_{\mathrm{cp}}}{2r^4} W_6\left(r; r_c^l\right), \tag{3}$$

was used, with the cutoff function W_6 defined as

$$W_6\left(r; r_c^l\right) = 1 - \mathrm{e}^{-(r/r_c^l)^6}, \tag{4}$$

and where $\alpha_1^l, \alpha_2^l, \alpha_3^l$ and r_c^l are l-dependent parameters optimised on the experimental energy levels of the singly-charged ion. Z is the charge of the nucleus and α_{cp} is the dipole polarisability volume of the doubly-charged ion. The values of the parameters $\alpha_1^l, \alpha_2^l, \alpha_3^l$ and r_c^l can be found in Ref. [69] for Mg and Ref. [33] for Sr. The spin-orbit interaction between the valence electrons and the screened nucleus is approximated by [33]

$$V^{\mathrm{SO}}_{slj}(r) = \frac{\alpha^2}{2}\vec{l}\cdot\vec{s}\,\frac{1}{r}\frac{\mathrm{d}V_l}{\mathrm{d}r}\left[1 - \frac{\alpha^2}{2}V_l(r)\right]^{-2}, \tag{5}$$

where α is the fine-structure constant. The bielectronic core-polarisation term $V^{(2)}_{\mathrm{pol}}(\boldsymbol{r_1},\boldsymbol{r_2})$ gives important corrections to the energies and widths of low-lying singly- and doubly-excited states of the heavier elements [68,70,71]. The corresponding matrix element, associated with the $l_1 j_1, l_2 j_2$ and $l_1' j_1', l_2' j_2'$ configurations, is given by

$$V^{(2)}_{\mathrm{pol}}(\boldsymbol{r_1},\boldsymbol{r_2}) = -\frac{\alpha_{\mathrm{cp}}}{r_1^2 r_2^2} P_1(\cos\theta_{12})\left[W_6(r_1; r_c^{l_1}) W_6(r_1; r_c^{l_1'}) \times W_6(r_2; r_c^{l_2}) W_6(r_2; r_c^{l_2'})\right]^{1/4}, \tag{6}$$

where θ_{12} represents the relative angle between $\boldsymbol{r}_1$ and $\boldsymbol{r}_2$ and r_c^l is the cutoff radius already present in Equations (3) and (4).

The solution of the time-independent two-electron Schrödinger equation

$$\hat{H}(\boldsymbol{r_1},\boldsymbol{r_2})\Psi(\boldsymbol{r_1},\boldsymbol{r_2}) = E\Psi(\boldsymbol{r_1},\boldsymbol{r_2}) \tag{7}$$

in the regions of phase space corresponding to singly-excited-, core-excited- and doubly-excited Rydberg states is difficult because of the large spatial extension of the electronic wavefunctions and the necessity to accurately treat electronic correlations over large distances. A number of theoretical approaches have been developed to tackle this problem and are briefly reviewed in the following sections.

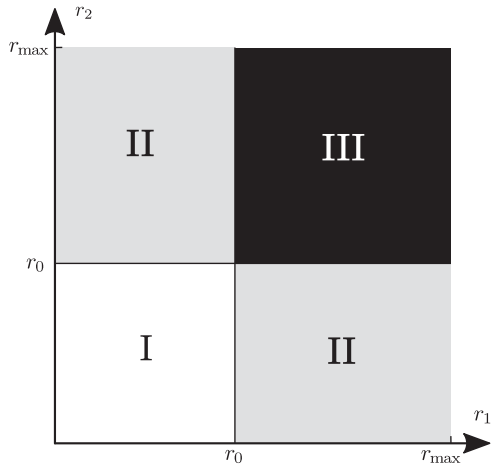

Figure 2. Schematic representation of the two-electron radial configuration space and the different regions (I, II and III) used in phase-space-partitioning strategies (see text).

2.1. Multichannel approaches

In singly- and core-excited Rydberg states, a natural partition occurs in the two-electron phase space because of the largely different radial extents of the motion of the core and Rydberg electrons ($\langle r_2 \rangle \gg \langle r_1 \rangle$ or vice versa, see Figure 2). The separation between the short- and long-range dynamics is at the heart of multichannel approaches, among which multichannel quantum-defect theory (MQDT) [30,33,72,73] was extensively used to study the Rydberg states of alkaline-earth metal atoms [33]. Following MQDT, the phase space is partitioned into two distinct regions (regions I and II in Figure 2). In the exterior region (region II), one of the two electrons evolves far away from the nucleus while the second valence electron remains close to the core (*i.e.* $r_2 \geq r_0$ and $r_1 < r_0$ or vice versa). It is assumed that the outer (Rydberg) electron experiences only the pure Coulomb field of the singly-charged ionic core, and any other interaction with the second valence electron is neglected. Within this approximation, the wave function describing the motion of the Rydberg electron in the outer region is known analytically. The associated orbital- and total-angular-momentum quantum numbers l_2 and j_2 are good quantum numbers. Along with the quantum numbers specifying the state of the ionic core (n_1, l_1, j_1), they are used to label the *channels*. In the inner region ($r_1, r_2 < r_0$, region I), both valence electrons are close to the nucleus. Their mutual interaction is nonnegligible and must be accounted for. The total angular momentum J of the two-electron system is a good quantum number but channels with different independent-electron quantum numbers n_1, l_1, j_1, l_2 and j_2 interact through the electron-electron repulsion ($1/r_{12}$ in Equation (2)), thereby inducing *channel mixing*. The penetration of the Rydberg electron wave function in the inner region is described in MQDT as the scattering of the Rydberg electron off the singly-charged ion core. The interaction between channels is then conveniently expressed in terms of the R matrix (or equivalently the K matrix) widely used in scattering theory [33]. In MQDT, it is assumed that one of the two electrons always remains close to the core, therefore the amplitude of the two-electron wave function in Region III of Figure 2 is always assumed to be negligible.

Channel-interaction parameters in MQDT can be either fitted to reproduce experimental energies or calculated theoretically [31,33,37–39]. The former approach is useful when the number of channels is relatively small and a theoretical description of the ionic core challenging (see Ref. [36] for a recent example). However, as the number of channels increases it becomes rapidly cumbersome, in particular because the fit results are not necessarily unique. The calculation of channel couplings from first principles, usually in the form of the R matrix, can be carried out by solving the complete two-electron Schrödinger equation in the inner region *only* [33]. This strongly reduces the computational cost of solving Equation (7) and makes it possible to describe ionic cores with more than one valence electron using state-of-the-art atomic-structure theory (see, *e.g.* Miecznik and Greene [74]). Moreover, the R matrix needs to be calculated only once and, by subsequent application of MQDT, a large number of physical quantities such as photoionisation cross sections and the energies and widths of entire singly-excited and core-excited Rydberg series can be obtained.

Several other multichannel methods have been developed to account for higher-order electrostatic interactions between the core and Rydberg electrons in the outer region [67,75]. They rely on the numerical propagation of the R matrix in the outer region, where only exchange is neglected, using a close-coupling scheme. The propagation results are then matched to analytic asymptotic boundary conditions, thereby yielding the desired physical quantities such as scattering phase shifts and scattering amplitudes. Whereas these methods were extensively used to study relatively low-lying doubly-excited Rydberg states of alkaline-earth metals observed in photoionisation experiments from the electronic ground state [8,10,76,77], they were seldom applied to the treatment of higher-lying singly- and core-excited Rydberg states [67].

In multichannel methods, an explicit calculation of the two-electron wave function in the entire phase space is usually avoided and the desired scattering quantities are obtained directly, *e.g.* from the R matrix. However, the calculation of observables relevant for studying two-electron dynamics, such as charge densities or

interelectronic angles, is best carried out from the two-electron wave function itself, which is not straightforward with multichannel approaches. For the same reason, it is also difficult to calculate the photoionisation cross section from an initial state with a wave function extending into the outer region, a situation that is encountered in the studies of ICE spectra of alkaline-earth metal atoms (green arrows in Figure 1). An independent-electron approach, the ICE approximation [78], was widely used to overcome this problem and provided relative photoionisation cross sections in good agreement with experimental data for low-lying core excitations. However, its reliability decreases with increasing core excitation (see Ref. [22] for an illustrative example). It is, in fact, the partitioning of phase space between short- and long-range dynamics that becomes inadequate as the degree of excitation of the core electron increases. Electron-electron correlations extend over larger radial distances and the distinction between 'core' and 'Rydberg' electrons becomes problematic. To take this into account, the radius r_0 of the inner region in multichannel calculations would have to be increased. However, the convergence of R-matrix MQDT calculations rapidly deteriorates with the size of the inner region [33], making an alternative technique desirable.

2.2. Direct approaches

The direct solution of the two-electron Schrödinger equation, without approximation and over large regions of phase space, was attempted in numerous works (see Ref. [2] and references therein). In these 'direct' approaches, electronic correlations are treated to all orders in the entire phase space (regions I, II and III in Figure 2), which makes them computationally much more intensive than multichannel approaches.

Spectral representations of two-electron wave functions in perimetric coordinates or using Hyleraas-type two-electron functions are known to describe two-electron bound states very accurately [79–82]. Simpler configuration-interaction expansions also perform well but exhibit slower convergence [83–85]. The use of (truncated) basis-set expansions to describe resonance states, *i.e.* bound states coupled to continua, is not straightforward because, unlike true bound states, their wave functions are not square integrable. This difficulty can be overcome using the method of complex scaling [86–90], in which the radial coordinates of each electron is artificially rotated away from the real axis into the complex plane by an angle θ ($\theta > 0$),

$$r \to r\mathrm{e}^{\mathrm{i}\theta}. \tag{8}$$

Using this procedure, continuum functions, which are not square-integrable for real r values, become exponentially damped at large radial distances and can be represented by square-integrable functions. Consequently, bound and continuum functions can be treated on the same footing, and a spectral expansion of the two-electron wave function can be carried out using a single discrete L^2 basis set. Successful applications of complex scaling to study doubly-excited Rydberg states of helium include basis-set expansions in perimetric coordinates [46,53,91,92], using Hyleraas-type two-electron functions [93,94] and configuration-interaction methods [84,95–99].

Nearly complete L^2 basis sets are required for complex scaling to work [100], making the solution of the two-electron Schrödinger equation very intensive computationally. As a result, complex-scaling methods have primarily been used to study relatively low-lying Rydberg states ($n \lesssim 20$) [6,46,53,84,96–99,101] but not, for example, high-lying core-excited Rydberg states. These methods typically neglect relativistic effects such as the spin-orbit interaction, which is very small in light two-electron systems such as He or H^-, and thus rely on the LS angular-momentum coupling scheme. In contrast, the spin-orbit interaction can be large in alkaline-earth metal atoms and must be taken into account to describe core-excited Rydberg states correctly [33]. Therefore, approaches computationally less intensive than those presented above are needed to study the high-lying doubly-excited Rydberg states of alkaline-earth metals.

2.3. Exterior-complex-scaling approach

In complex scaling, *both* single- and double-ionisation processes are naturally accounted for because the radial coordinates of both electrons are rotated into the complex plane. The fact that double ionisation is suppressed below the double-ionisation threshold can be exploited, in a second 'partition' of phase space, to reduce the computational complexity of the direct methods presented in the previous section. In this approach, referred to as exterior complex scaling (ECS) [102], the radial coordinates of both electrons are also rotated into the complex plane, but only beyond a certain radius r_0,

$$r \to \begin{cases} r & \text{if } r < r_0, \\ r_0 + (r - r_0)\mathrm{e}^{\mathrm{i}\theta} & \text{if } r \geq r_0. \end{cases} \tag{9}$$

For the problems considered in this article, the motion of at least one of the two electrons is confined to finite radial distances, and one can choose r_0 such that this electron evolves in the region where complex scaling has not

been applied ($r < r_0$). A nearly complete L^2 basis set is no longer required for this electron but, instead, a small number of real basis functions suffices. The amplitude of the two-electron wave function in region III of Figure 2 ($r_1, r_2 > r_0$) is assumed to be negligible. The approximation of describing one of the two electrons with a limited set of core basis functions is much less stringent than the approximations on which, *e.g.* *R*-matrix MQDT relies (see Section 2.1). The requirement of basis completeness for only one electron, instead of two electrons in the direct approaches described Section 2.2, greatly reduces the size of the basis set. As a consequence, Rydberg states with much larger principal quantum numbers can be described while treating electron-electron correlations to all orders everywhere. The ECS radius is chosen according to the problem, with r_0 being small for core-excited Rydberg states and larger for higher-lying doubly-excited Rydberg states. The flexibility of ECS makes it attractive for a broad range of problems, some aspects of which were reviewed by Moiseyev [103,104] and McCurdy *et al.* [105]. Recent examples include electron scattering [106–108], double photoionisation [109,110], molecular dissociation [111–113], dissociative recombination [114,115], field ionisation [116], photoionisation [117] and high-harmonic generation [118].

ECS permits, together with basis-set-expansion techniques, the explicit calculation of the (complex-scaled) two-electron wave function. Consequently, observables relevant for studying two-electron dynamics, such as the interelectronic angle, can be evaluated directly. Absolute photoionisation cross sections from Rydberg states, where one of the two electrons is already in the outer region ($r \geq r_0$), can be evaluated using procedures identical to those used for photoionisation from the ground electronic state ($r_1, r_2 < r_0$) [119]. In contrast to standard complex scaling, quantities such as photoionisation branching ratios and photoelectron angular distributions can be calculated directly by taking advantage of the fact that, in the inner region ($r < r_0$), the radial coordinates are real and thus physically meaningful [117,120,121].

2.4. Configuration interaction with exterior complex scaling

ECS, combined with a basis-set expansion of the two-electron wave function, appears well suited to investigate doubly-excited Rydberg states in quasi-two-electron systems. We describe below in some detail the configuration-interaction-with-exterior-complex-scaling (CI-ECS) approach that we use to study doubly-excited Rydberg states of alkaline-earth metal atoms (see also Refs. [119,122]), building on the early work of Fields *et al.* in Sr [123].

The two-electron wave function is expanded in a set of antisymmetrised products of two one-electron wave functions,

$$\Psi^{\pi}_{JM}(\boldsymbol{r}_1, \boldsymbol{r}_2) = \sum_{n_1,l_1,j_1} \sum_{n_2,l_2,j_2} C^{J}_{n_1 l_1 j_1 n_2 l_2 j_2} \times \mathcal{A}\left[\frac{u_{n_1 l_1 j_1}(r_1)}{r_1} \frac{u_{n_2 l_2 j_2}(r_2)}{r_2} \Lambda^{JM}_{l_1 j_1 l_2 j_2}(\hat{\boldsymbol{r}}_1, \hat{\boldsymbol{r}}_2) \right], \quad (10)$$

where n_i, l_i and j_i ($i = 1, 2$) denote the principal-, orbital- and total-angular-momentum quantum numbers of the electrons, J and M are the total-angular-momentum and magnetic quantum numbers of the two-electron system and π is the parity of the total wave function. The summations over l_1 and l_2 run such that the basis functions have the correct parity π and the summations over n_1, l_1, j_1, n_2, l_2 and j_2 are carried out such that each configuration appears only once in the expansion. $C^{J}_{n_1 l_1 j_1 n_2 l_2 j_2}$ represent expansion coefficients and $\mathcal{A}$ is the antisymmetrisation operator. The normalisation factor $1/\sqrt{2(1+\delta_{n_1 n_2}\delta_{l_1 l_2}\delta_{j_1 j_2})}$ of each basis function is assumed to be included in the expansion coefficient. The one-electron radial wave functions are denoted by $u_{n_i l_i j_i}(r)/r$ and the two-electron angular- and spin wave function $\Lambda^{JM}_{l_1 j_1 l_2 j_2}(\hat{\boldsymbol{r}}_1, \hat{\boldsymbol{r}}_2)$ is built from one-electron spherical harmonics and spinors using standard angular-momentum algebra [124]. The configuration-interaction expansion in Equation (10) is written in the *jj*-coupling scheme, which is appropriate when the spin-orbit interaction is large (see Ref. [33] for a detailed discussion), as is often the case for core-excited Rydberg states of alkaline-earth metal atoms.

The radial functions $u_{nlj}(r)$ are chosen to be the solutions of the one-electron reduced radial equation,

$$\left(-\frac{1}{2}\frac{\mathrm{d}^2}{\mathrm{d}r^2} + \frac{l(l+1)}{2r^2} + V_l(r) + V^{\mathrm{so}}_{slj}(r) - \epsilon_{nlj} \right) \times u_{nlj}(r) = 0, \quad (11)$$

describing the radial motion of the valence electron of the singly-charged ion. The solution must be calculated along the ECS contour defined in Equation (9). The differential equation (11) is solved in a 'box' ($r \leq r_{\max}$) and subject to the boundary conditions that $u_{nlj}(r)$ vanishes at both ends of the box ($r = 0$ and $r = r_{\max}$). The functions $u_{nlj}(r)$ are thus square integrable, but can represent equally well bound states ($\epsilon_{nlj} < 0$) and continuum states ($\epsilon_{nlj} \geq 0$) because of ECS. The box size $r_{\max}$ sets a limit to the highest-n Rydberg wave function

that can be accurately represented, which corresponds to the situation where the classical outer turning point of the Rydberg-electron motion, $r = \frac{2n^2}{Z}$, is comparable to $r_{\max}$ [125].

In the ECS contour given in Equation (9), the transition between the inner region and the outer complex-rotated region is sharp and introduces a discontinuity in the derivative of the radial function at the ECS radius. Its accurate representation requires the use of functions with compact support (*e.g.* piecewise polynomials) [105]. For this purpose we use the finite-element discrete-variable-representation (FEM-DVR) approach of Rescigno and McCurdy [126]. The one-dimensional r space is partitioned into several contiguous but non-overlapping finite elements, and one of the boundaries is chosen to lie at the ECS radius r_0. Within each element, Equation (11) is solved on a numerical grid using a DVR approach similar to that introduced by Manolopoulos and Wyatt [127], which is based on the Gauss-Lobatto quadrature. The continuity of the solution $u_{nlj}(r)$ across the element boundaries is enforced, but *not* the continuity of its derivatives, so that the discontinuity at the ECS radius is correctly represented. Other approaches to ECS have also been developed, *e.g.* using B-splines [105,128–130] or analytic functions together with a smooth transition between the inner and outer regions [131,132], but they have not been followed in the present work.

The present DVR approach, analogous to the Legendre pseudospectral method [133,134], converges very rapidly with the number of grid points. Accurate energies and wave functions can be obtained with even modest grid sizes [125,133], and the computation of matrix elements involving these wave functions can be carried out using the underlying Gauss-Lobatto quadrature without loss of accuracy. Moreover, the finite-element aspect of the FEM-DVR approach allows considerable flexibility in the definition of the overall radial grid and permits, after optimisation, a significant reduction of the number of grid points while preserving the accuracy of the results. In our experience, placing a small element with a large grid-point density close to the core and a larger element with smaller grid-point density further away is a reliable starting point. For example, we could obtain the energies of $Mg^+(nl_j)$ states with $n \leq 90$ converged to within 10^{-13} Hartree using two elements spanning the ranges $[0, 100]\, a_0$ and $[100, 17{,}600]\, a_0$, respectively, and containing 101 and 551 grid points each (see Ref. [119]). In the calculations in Sr presented in Section 3.2, further optimisation was required to minimise the grid size, and a third element was inserted between the two others, yielding the elements $[0, 10]\, a_0$, $[10, 150]\, a_0$, and $[150, 1350]\, a_0$, with 70, 60 and 80 grid points, respectively. In this way, accurate energies of $Sr^+(nlj)$ states ($n \leq 36$) were obtained with 208 grid points only, with a convergence of better than 10^{-9} Hartree except for a few low-lying np states which could be described with an accuracy of $\sim 10^{-6}$ Hartree or better.

The calculation of the matrix elements of the two-electron Hamiltonian given in Equation (2) is carried out with the configuration-interaction basis set of Equation (10). The one-electron part (first six terms on the right-hand side of Equation (2)) is easily calculated because the total wave function is built from one-electron spin-orbitals. The calculation of the matrix elements associated with the bielectronic repulsion $1/r_{12}$ relies on the multipole expansion

$$\frac{1}{r_{12}} = \sum_q \frac{r_<^q}{r_>^{q+1}} P_q(\cos\theta_{12}), \tag{12}$$

where $r_< = \min(r_1, r_2)$ and $r_> = \max(r_1, r_2)$. The associated angular integrals can be calculated using standard angular momentum algebra [124] whereas the radial integrals must be calculated numerically, *e.g.* as described in Refs. [105,119]. The matrix elements of the bielectronic core polarisation operator $V_{\text{pol}}^{(2)}(\boldsymbol{r_1}, \boldsymbol{r_2})$ are obtained directly from Equation (6). The angular integrals are identical those for the $q = 1$ term of the multipole expansion of $1/r_{12}$, and the radial integrals are calculated numerically from the one-electron radial functions $u_{nlj}(r)$ using the Gauss-Lobatto quadrature underlying the FEM-DVR method.

The two-electron Hamiltonian matrix is complex-symmetric, dense and typically large. For the calculations of core-excited Rydberg states of Mg reported in Ref. [119], matrix sizes of around 15,000 × 15,000 were used for a given total parity π and a given value of J, which is still small enough to be diagonalised using standard numerical linear-algebra libraries. For the calculations of higher-lying doubly-excited, such as those of Sr presented in Section 3.2, matrix sizes reach up to 80,000 × 80,000. Since, in most cases, only a small subset of the eigenvalue spectrum is desired, iterative diagonalisation algorithms are advantageous and significantly reduce the computational effort. We have used the standard Lanczos algorithm [135] and its thick-restart variant [136], adapted to complex-symmetric matrices, with equal success.

3. Selected examples

3.1. Core-excited Rydberg states

The core-excited Rydberg states of alkaline-earth metal atoms have been extensively studied both experimentally and theoretically (see Ref. [33] and references therein), and thus represent ideal systems to test the CI-ECS

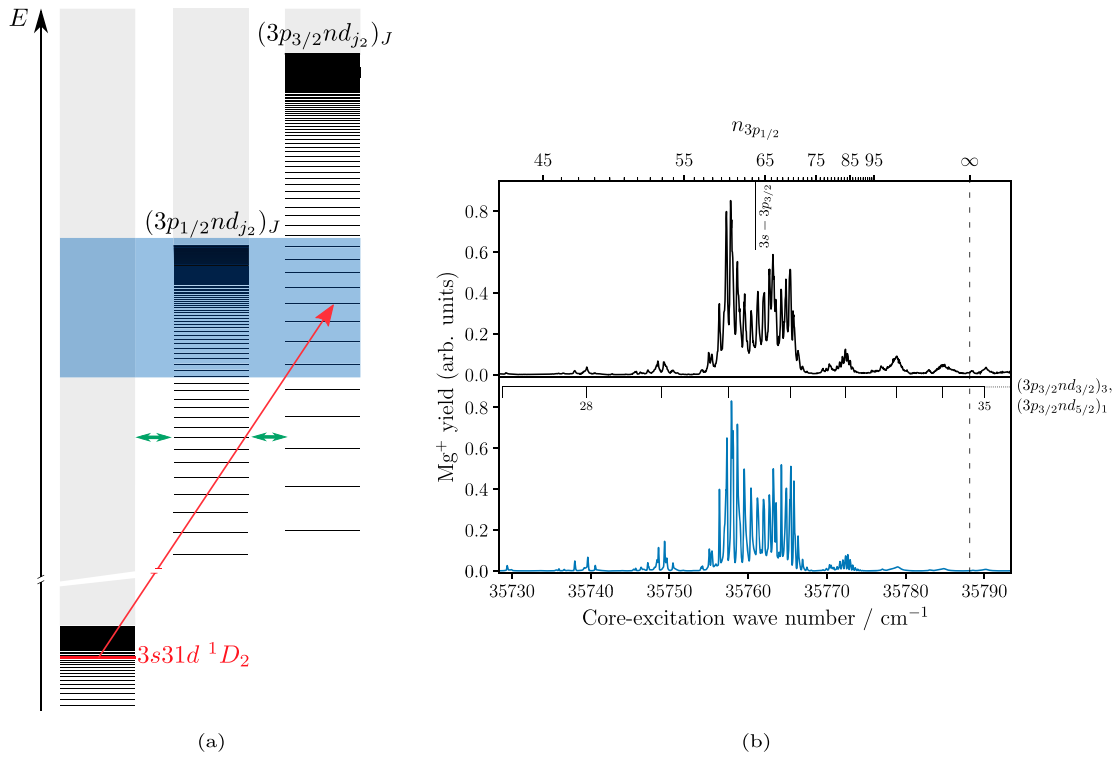

Figure 3. (a) Schematic view of the energy-level structure of the $3snd\ ^1D_2$ singly-excited Rydberg states and $(3p_{j_1}nd_{j_2})_J$ core-excited Rydberg states of Mg. The green arrows denote channel interactions. The red arrow depicts the isolated core excitation. The shaded blue area is the energy range probed in the spectra shown in panel (b). (b) Experimental (top) and theoretical (bottom) isolated-core-excitation spectra from the $3s31d\ ^1D_2$ state of Mg in the vicinity of the $3s - 3p_{3/2}$ core transition. The position of the Mg$^+$($3s - 3p_{3/2}$) transition is shown by the full vertical line in the upper panel. The positions of $(3p_{3/2}nd_{j_2})_J$ resonances are shown in the assignment bar in the lower panel. Values of the principal quantum numbers $n_{3p_{1/2}}$ calculated relative to the Mg$^+$($3p_{1/2}$) threshold (dashed vertical line) are shown in the assignment bar in the upper panel. Adapted with permission from Génévriez *et al.* [119].

method. In an early study, Fields *et al.* used an approach analogous to CI-ECS to calculate the quantum defects and autoionisation rates of the $5pnp$ and $5pnf$ core-excited Rydberg states of Sr, obtaining good agreement with available experimental data [123]. Recently, we used the CI-ECS method to estimate the autoionisation rates of fully-Stark-mixed high-lying core-excited Rydberg states of Mg converging to the Mg$^+$($3p_{3/2}$) threshold, obtaining excellent agreement with experimental observations [122].

A stringent test of the accuracy of theoretical predictions consists in the comparison between theoretical and experimental ICE spectra. These spectra correspond to the photoexcitation spectrum from Rydberg states with the core in its ground state to core-excited Rydberg states (see, *e.g.* Ref. [137] for a detailed discussion). The core-excited Rydberg states rapidly autoionise and, in the experiments, the ion yield is recorded as a function of the core-excitation laser frequency. An example, taken from Ref. [119], is shown in Figure 3 and corresponds to the ICE spectrum from the $3s31d\ ^1D_2$ Rydberg state of Mg in the vicinity of the $3s_{1/2} - 3p_{3/2}$ core-excitation resonance. Overall, the positions and shapes of the autoionizing resonances in the experimental spectrum (upper panel of Figure 3(b)) are very well reproduced by the calculation (lower panel). The spectra consist of broad lines, associated with states having predominant $3p_{3/2}nd$ character and principal quantum numbers similar to that of the initial state ($n \simeq 27$–35, see assignment bar in the lower panel), on top of which a progression of closely-spaced sharp resonances is superimposed. Inspection of the CI coefficients reveals that these sharp resonances are associated with states of predominant $3p_{1/2}n'd$ character and significantly larger principal quantum numbers (see assignment bar in the upper panel). Because the photon energy is far detuned from the $3s_{1/2} - 3p_{1/2}$ resonance, a direct excitation of $3p_{1/2}n'd$ states is very unlikely. Their presence in the spectrum is rather the result of the mixing with $3p_{3/2}nd$ states caused by electron-electron correlations. The overall intensity distribution of the experimental spectrum is also well reproduced by the theoretical calculation. It is governed predominantly by the immediate response of the Rydberg electron to the excitation of the core, *i.e.* within the

independent-electron approximation, by the modification of the Rydberg electron wave function caused by the change of the ionic-core properties [14,137].

Excellent agreement between theory and experiment was found for all other spectra recorded in Mg up to $n \simeq 80$ [119], to a level similar to those of R-matrix MQDT calculations performed for similar states [17,42]. This level of agreement shows that the CI-ECS method can compete with state-of-the-art methods in describing core-excited Rydberg states accurately, and makes us confident that higher-lying doubly-excited states can also be studied.

3.2. Breakdown of the independent-electron approximation: 'dipole-forbidden' core excitation

With increasing excitation of the core electron, the independent-electron approximation is expected to break down. A particularly illustrative example of this situation is the observation of core excitations that would be dipole forbidden if the core were strictly isolated from the Rydberg electron [16,18,22]. For instance, Huang *et al.* have recorded spectra corresponding to the one-photon excitation of the core electron from the $5d_{5/2}$ to the $7d_{5/2}$ orbital in Sr, in the presence of a Rydberg electron initially in the $n = 16$, $l = 14$ state [22]. A one-electron transition with $\Delta l = 0$ is dipole-forbidden because of parity. In order for the $5d_{5/2} - 7d_{5/2}$ core excitation to occur, the Rydberg electron must thus change angular momentum, which can happen only if electron-electron correlations are sufficiently large. The core excitation caused by nondipole transitions is negligible. To the best of our knowledge, no calculation from first principles has been attempted to reproduce the experimental results of Ref. [22].

We carried out a calculation of the core-excitation spectrum using the eigenvectors of the two-electron Hamiltonian calculated with the FEM-DVR grid described in Section 2.4, for which complex rotation was applied for $r \geq 150\,a_0$ with an angle of 10°. The ∼80,000 two-electron CI-ECS basis functions were built from (i) all orbitals with energies lower than the $Sr^+(11s)$ state to describe the 'inner' electron and (ii) the complete set of 208 radial functions from the one-electron FEM-DVR calculations to describe the 'outer' electron. In order to reproduce the experimental spectrum, the populations of the various initial states, labelled in the *jj* coupling scheme by $(5d_{5/2}16(l = 14)_{j_2})_J$ with $j_2 = \frac{27}{2}, \frac{29}{2}$ and $J = 12$, 14 and 16, must be estimated. These states were prepared by two-photon excitation from the $5s16(l = 14)$ singlet state [22]. A complete simulation of the preparation process can in principle be carried out using CI-ECS, but this goes beyond the scope of this article. Instead, the relative populations were estimated using a simple independent-electron picture [124] and assuming that the radial integrals of the transition matrix elements are independent of j_2. We found values of 0.33, 0.075 and 0.095 for the states with $j_2 = \frac{29}{2}$ and $J = 12$, 14 and 16, respectively, and values of 0.065, 0.08, and 0.355 for those with $j_2 = \frac{27}{2}$ and $J = 12$, 14 and 16. The theoretical wave numbers were corrected by the difference (∼26 cm^{-1}) between the calculated $Sr^+(5d_{5/2}) - Sr^+(7d_{5/2})$ excitation wave number and its experimental value [138].

The $5d_{5/2}16(l = 14) - 7d_{5/2}n'l'$ excitation spectrum recorded by Huang *et al.* [22] is compared in Figure 4 to the theoretical spectrum calculated using the CI-ECS method. The experimental spectrum represents the Sr^{2+} yield after excitation of Sr atoms to $7d_{5/2}n'l'$ states and subsequent photoionisation, field ionisation, autoionisation or any combination thereof. The theoretical spectrum is obtained from the core-excitation cross section only, which is convoluted by a Gaussian function with a full width at half maximum of 0.25 cm^{-1}, a value within the range of the typical bandwidth of the pulsed dye lasers used in Ref. [22]. Discrepancies between the intensities of the measured and calculated lines can thus be attributed to differences in the Sr^{2+} production efficiency from the different $7d_{5/2}n'l'$ states, because the various double-ionisation mechanisms in the experiment are known to depend on n' but this dependence is not accounted for in the theoretical spectrum, or inaccuracies of the theoretical treatment. Moreover, stray electric fields in the experiment can cause l values of the Rydberg electron other than $l = 14$ to be populated [62], which leads to the appearance of additional lines in the experimental spectra. The autoionisation widths of all states contributing to the spectrum are calculated to be smaller than $\sim 10^{-9}$ Hartree (∼0.0002 cm^{-1}). The widths of the lines are thus predominantly caused by the spectral width of the laser.

The agreement between the experimental and theoretical spectra is good. The most intense lines lie at lower wave numbers than would be expected in the absence of electron-electron correlations (red lines in Figure 4), indicating a nonzero quantum defect. This is in contrast with the behaviour expected for high-l singly-excited or core-excited Rydberg states, for which quantum defects are very close to zero. The jump in the quantum defect between $n < 16$ and $n > 16$ originates from the change of the orbital-angular-momentum quantum number l' of the Rydberg electron in the final state from 13 to 15 (see assignment bar in Figure 4). This fact, and the obvious absence of the $n = 16$ line in the spectrum, were discussed in the light of a perturbative configuration-interaction model in Ref. [22], which qualitatively reproduced the observed lines intensities. It was postulated

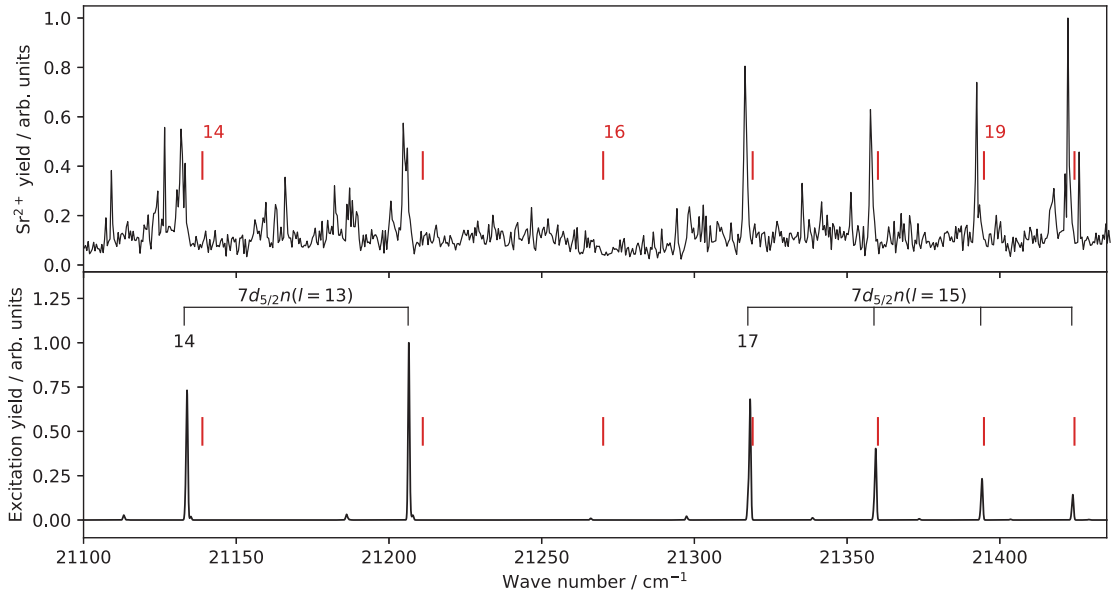

Figure 4. Experimental (top) and theoretical (bottom) spectra of the $5d_{5/2}16(l = 14) - 7dn'l'$ transitions in Sr. The vertical red lines show the expected positions of $7dn'l'$ states in the *absence* of electron-electron correlations, and are labelled with the values of n'. The assignment bars in the bottom panel attribute the strongest resonances to the relevant $7d_{5/2}n'l'$ states. The weak lines, red shifted from the strong ones, correspond to $7d_{3/2}n'l'$ states. The experimental spectrum is taken from Ref. [22].

that the dipole excitation from the $5d_{5/2}16(l = 14)$ state to $7d_{5/2}n'l'$ states is made possible by the admixture of $6f_{7/2}16(l = 14)$ character in the latter states, caused by the dipole term of the bielectronic interaction ($q = 1$ in Equation (12)). The mixing with $8p_{3/2}16(l = 14)$ is also possible, however it does not play an important because the $5d_{5/2} - 8p_{3/2}$ transition dipole moment is very small. The present CI-ECS calculation confirms these observations and further shows the admixture of $6p_{3/2}16(l = 14)$ character to the $5d_{5/2}16(l = 14)$ initial state which significantly contributes to the overall transition dipole matrix element. Therefore, the spectra in Figure 4 are the results of correlations in both the initial and the final state.

4. Conclusion and perspectives

In this article, we presented the CI-ECS method and its use for studying doubly-excited Rydberg states of quasi-two-electron systems. The method does not rely on the approximations of *R*-matrix MQDT, widely used to study core-excited Rydberg states of alkaline-earth metals, because it treats electron-electron correlations to all orders everywhere. It is expected to provide accurate results even for doubly-excited Rydberg states in which both electrons are highly excited, a situation where *R*-matrix MQDT is not applicable. CI-ECS computations are also significantly less intensive than those based on the direct solution of the two-electron Schrödinger equation using basis-set-expansion techniques in combination with complex scaling, because CI-ECS allows one to limit the description of one of the two valence electrons to a small number of basis functions. Consequently, core-excited Rydberg states with principal quantum numbers as high as $n \simeq 100$ can be calculated while, at the same time, taking the spin-orbit interaction into account. In comparison, direct methods are limited to $n \lesssim 20$ and neglect spin-orbit interaction [97]. The CI-ECS method thus appears ideally suited to study, from first principles, a broad range of Rydberg states at once: singly-excited-, core-excited- and higher-lying doubly-excited Rydberg states, the energies, autoionisation rates and wave functions of which can be calculated through the diagonalisation of a single, large Hamiltonian matrix. ICE spectra from $3snd$ singly-excited Rydberg states of Mg to $3pnd$ core-excited Rydberg states were calculated and excellent agreement with experimental data was obtained (see also Ref. [119]). The use of CI-ECS to treat higher-lying doubly-excited states was demonstrated in a calculation of the one-photon excitation spectrum from the $5d16(l = 14)$ state of Sr to $7dn'l'$ states ($n' \leq 20, l' = 13 - 15$), a process only possible because of the presence of electronic correlations. Excellent agreement was obtained with available experimental data [22].

The CI-ECS approach opens interesting perspectives in the study of correlated two-electron motion in alkaline-earth metal atoms. The transfer of the theoretical concepts developed for the helium atom [2] to quasi-two-electron systems is only possible through systematic comparisons between model predictions and well-converged two-electron wave functions, as provided

by the CI-ECS method. A question of particular interest is whether frozen-planet states [52,53], one of the most important modes of collective two-electron motion in helium [2], are encountered in alkaline-earth metal atoms. The extent by which two-electron frozen-planet states are perturbed by their interaction with the Mg^{2+}-core electrons is unknown. Such states were never observed in helium because of their very small photoexcitation probability from the ground state [13], however excitation schemes to doubly-excited Rydberg states of alkaline-earth metal atoms are far more flexible because of the smaller photon energies involved. CI-ECS calculations are well suited to search for frozen-planet states and, possibly, to design a suitable excitation scheme.

Rydberg-based quantum computing and quantum simulation with alkaline-earth metal atoms relies on high Rydberg-detection fidelities which, in some experiments, depend on the excitation dipole moments to core-excited Rydberg states and on their autoionisation rates [27]. Such quantities can be calculated using CI-ECS and their knowledge is desirable to select, in current and future experiments, the most suitable core-excited Rydberg states. The production of core-excited Rydberg states that are metastable against autoionisation is actively pursued in the context of Rydberg-atom trapping and manipulation [26,28,29], and typically relies on increasing the orbital-angular-momentum quantum number l of the Rydberg electron. The l-dependence of the autoionisation rates of core-excited Rydberg states is not well understood, and a theoretical investigation of the subject using CI-ECS is under way.

From a theoretical perspective, numerous possibilities exist to further develop the CI-ECS method. The computation of partial and differential photoexcitation and photoionisation cross sections from the values of the two-electron wave functions near the ECS radius [117,121] is a perspective of future work, and may prove challenging when the number of decay channels is very large. Improvements to the convergence of the spectral representation of the wave function with the number of basis functions must also be considered in order to be able to describe very-high-lying doubly-excited Rydberg states accurately with the finite resources of current computers [83,139]. Finally, the extension of the method to molecular systems is a major prospect. The rotational and vibrational motion of the ion core of a Rydberg molecule significantly complicates the problem compared to atoms. Also, the Born-Oppenheimer approximation is not applicable because the time scale of nuclear motion is comparable to, or shorter than, the time scale associated with the motion of an electron in a high Rydberg state. Nonetheless, such issues have been addressed with the development of molecular MQDT and R-matrix techniques [72,73,75] and similar strategies can be applied to CI-ECS. Interestingly, ECS is one of the rare techniques that can treat from first principles problems involving the simultaneous breakup of three bodies [105]. In the molecular context, the development of molecular CI-ECS would thus pave the way to investigating dissociative ionisation processes, which are notoriously challenging for theory [140].

Acknowledgments

The author gratefully acknowledges fruitful discussions with F. Merkt and D. Wehrli, and thanks U. Eichmann for providing the data files presented in Figure 4.

Disclosure statement

No potential conflict of interest was reported by the author(s).

ORCID

M. Génévriez http://orcid.org/0000-0002-0738-5033

References

[1] H.A. Bethe and E.E. Salpeter, *Quantum Mechanics of One- and Two-Electron Atoms* (Springer-Verlag Berlin Heidelberg, Berlin, Heidelberg, 1957).
[2] G. Tanner, K. Richter and J.M. Rost, Rev. Mod. Phys. **72**, 497 (2000). doi:10.1103/RevModPhys.72.497.
[3] C.D. Lin, Phys. Rep. **257**, 1 (1995). doi:10.1016/0370-1573(94)00094-J.
[4] C.H. Greene, P. Giannakeas and J. Pérez-Ríos, Rev. Mod. Phys. **89**, 035006 (2017). doi:10.1103/RevModPhys.89.035006.
[5] C. Ott, A. Kaldun, L. Argenti, P. Raith, K. Meyer, M. Laux, Y. Zhang, A. Blättermann, S. Hagstotz, T. Ding, R. Heck, J. Madroñero, F. Martín and T. Pfeifer, Nature **516**, 374 (2014). doi:10.1038/nature14026.
[6] M. Domke, K. Schulz, G. Remmers, G. Kaindl and D. Wintgen, Phys. Rev. A **53**, 1424 (1996). doi:10.1103/PhysRevA.53.1424.
[7] K. Schulz, G. Kaindl, M. Domke, J.D. Bozek, P.A. Heimann, A.S. Schlachter and J.M. Rost, Phys. Rev. Lett. **77**, 3086 (1996). doi:10.1103/PhysRevLett.77.3086.
[8] A. Czasch, M. Schöffler, M. Hattass, S. Schössler, T. Jahnke, T. Weber, A. Staudte, J. Titze, C. Wimmer, S. Kammer, M. Weckenbrock, S. Voss, R.E. Grisenti, O. Jagutzki, L.P.H. Schmidt, H. Schmidt-Böcking, R. Dörner, J.M. Rost, T. Schneider, C.N. Liu, I. Bray, A.S. Kheifets and K. Bartschat, Phys. Rev. Lett. **95**, 243003 (2005). doi:10.1103/PhysRevLett.95.243003.
[9] A. Menzel, S.P. Frigo, S.B. Whitfield, C.D. Caldwell, M.O. Krause, J.Z. Tang and I. Shimamura, Phys. Rev. Lett. **75**, 1479 (1995). doi:10.1103/PhysRevLett.75.1479.
[10] Y.H. Jiang, R. Püttner, R. Hentges, J. Viefhaus, M. Poygin, C. Cacho, U. Becker, J.M. Rost and G. Kaindl, J. Phys. B: At. Mol. Opt. Phys. **39**, L9 (2005). doi:10.1088/0953-4075/39/1/L02.

[11] B. Krässig, E.P. Kanter, S.H. Southworth, L. Young, R. Wehlitz, B.A. deHarak and N.L.S. Martin, Phys. Rev. A **86**, 053408 (2012). doi:10.1103/PhysRevA.86.053408.

[12] J.J. Jureta, A.R. Milosavljević and B.P. Marinković, Int. J. Mass Spectrom. **365-366**, 114 (2014). doi:10.1016/j.ijms.2014.03.002.

[13] Y.H. Jiang, R. Püttner, D. Delande, M. Martins and G. Kaindl, Phys. Rev. A **78**, 021401 (2008). doi:10.1103/PhysRevA.78.021401.

[14] W.E. Cooke, T.F. Gallagher, S.A. Edelstein and R.M. Hill, Phys. Rev. Lett. **40**, 178 (1978). doi:10.1103/PhysRevLett.40.178.

[15] F. Gounand, T.F. Gallagher, W. Sandner, K.A. Safinya and R. Kachru, Phys. Rev. A **27**, 1925 (1983). doi:10.1103/PhysRevA.27.1925.

[16] P. Camus, T.F. Gallagher, J.M. Lecomte, P. Pillet, L. Pruvost and J. Boulmer, Phys. Rev. Lett. **62**, 2365 (1989). doi:10.1103/PhysRevLett.62.2365.

[17] C.J. Dai, G.W. Schinn and T.F. Gallagher, Phys. Rev. A **42**, 223 (1990). doi:10.1103/PhysRevA.42.223.

[18] R.R. Jones and T.F. Gallagher, Phys. Rev. A **42**, 2655–2660 (1990). doi:10.1103/PhysRevA.42.2655.

[19] U. Eichmann, V. Lange and W. Sandner, Phys. Rev. Lett. **64**, 274 (1990). doi:10.1103/PhysRevLett.64.274.

[20] M.D. Lindsay, C.J. Dai, B.J. Lyons, C.R. Mahon and T.F. Gallagher, Phys. Rev. A **50**, 5058 (1994). doi:10.1103/PhysRevA.50.5058.

[21] P. Camus, Phys. Scr. **T51**, 20 (1994). doi:10.1088/0031-8949/1994/T51/003.

[22] W. Huang, C. Rosen, U. Eichmann and W. Sandner, Phys. Rev. A **61**, 040502 (2000). doi:10.1103/PhysRevA.61.040502.

[23] J. Millen, G. Lochead and M.P.A. Jones, Phys. Rev. Lett. **105**, 213004 (2010). doi:10.1103/PhysRevLett.105.213004.

[24] R. Mukherjee, J. Millen, R. Nath, M.P.A. Jones and T. Pohl, J. Phys. B: At. Mol. Opt. Phys. **44**, 184010 (2011). doi:10.1088/0953-4075/44/18/184010.

[25] J. Millen, G. Lochead, G.R. Corbett, R.M. Potvliege and M.P.A. Jones, J. Phys. B: At. Mol. Opt. Phys. **44**, 184001 (2011). doi:10.1088/0953-4075/44/18/184001.

[26] J. Wilson, S. Saskin, Y. Meng, S. Ma, R. Dilip, A. Burgers and J. Thompson, ArXiv191208754 Phys. Physicsquant-Ph (2019).

[27] I.S. Madjarov, J.P. Covey, A.L. Shaw, J. Choi, A. Kale, A. Cooper, H. Pichler, V. Schkolnik, J.R. Williams and M. Endres, Nat. Phys. **16**, 857–861 (2020). doi:10.1038/s41567-020-0903-z.

[28] H. Lehec, X. Hua, P. Pillet and P. Cheinet, ArXiv200509-552 Phys. Physicsquant-Ph (2020).

[29] R.C. Teixeira, A. Larrouy, A. Muni, L. Lachaud, J.M. Raimond, S. Gleyzes and M. Brune, ArXiv200615-921 Phys. Physicsquant-Ph (2020).

[30] M.J. Seaton, Rep. Prog. Phys. **46**, 167 (1983). doi:10.1088/0034-4885/46/2/002.

[31] U. Fano, Phys. Rev. A **2**, 353 (1970). doi:10.1103/PhysRevA.2.353.

[32] U. Fano, J. Opt. Soc. Am. **65**, 979 (1975). doi:10.1364/JOSA.65.000979.

[33] M. Aymar, C.H. Greene and E. Luc-Koenig, Rev. Mod. Phys. **68**, 1015 (1996). doi:10.1103/RevModPhys.68.1015.

[34] C.L. Vaillant, M.P.A. Jones and R.M. Potvliege, J. Phys. B: At. Mol. Opt. Phys. **47**, 155001 (2014). doi:10.1088/0953-4075/47/15/155001.

[35] M. Aymar and P. Camus, Phys. Rev. A **28**, 850 (1983). doi:10.1103/PhysRevA.28.850.

[36] H. Lehec, A. Zuliani, W. Maineult, E. Luc-Koenig, P. Pillet, P. Cheinet, F. Niyaz and T.F. Gallagher, Phys. Rev. A **98**, 062506 (2018). doi:10.1103/PhysRevA.98.062506.

[37] C.M. Lee and W.R. Johnson, Phys. Rev. A **22**, 979 (1980). doi:10.1103/PhysRevA.22.979.

[38] W.R. Johnson, K.T. Cheng, K.N. Huang and M. Le Dourneuf, Phys. Rev. A **22**, 989 (1980). doi:10.1103/PhysRevA.22.989.

[39] K.T. Lu, Phys. Rev. A **4**, 579 (1971). doi:10.1103/PhysRevA.4.579.

[40] T.F. Gallagher, *Rydberg Atoms* (Cambridge University Press, Cambridge, 1994).

[41] V.L. Sukhorukov, I.D. Petrov, M. Schäfer, F. Merkt, M.W. Ruf and H. Hotop, J. Phys. B: At. Mol. Opt. Phys. **45**, 092001 (2012). doi:10.1088/0953-4075/45/9/092001.

[42] G.W. Schinn, C.J. Dai and T.F. Gallagher, Phys. Rev. A **43**, 2316 (1991). doi:10.1103/PhysRevA.43.2316.

[43] E.Y. Xu, Y. Zhu, O.C. Mullins and T.F. Gallagher, Phys. Rev. A **35**, 1138 (1987). doi:10.1103/PhysRevA.35.1138.

[44] R.R. Jones, P. Fu and T.F. Gallagher, Phys. Rev. A **44**, 4260 (1991). doi:10.1103/PhysRevA.44.4260.

[45] D.R. Herrick, in *Advances in Chemical Physics*, edited by I. Prigogine and S.A. Rice, Vol. LII (John Wiley & Sons, Ltd, New York, 1983), pp. 1–115.

[46] A. Burgers, D. Wintgen and J.M. Rest, J. Phys. B: At. Mol. Opt. Phys. **28**, 3163 (1995). doi:10.1088/0953-4075/28/15/010.

[47] K. Richter, G. Tanner and D. Wintgen, Phys. Rev. A **48**, 4182 (1993). doi:10.1103/PhysRevA.48.4182.

[48] M.C. Gutzwiller, *Chaos in Classical and Quantum Mechanics*, *Interdisciplinary Applied Mathematics*, Vol. 1 (Springer New York, New York, NY, 1990).

[49] J. Müller, X. Yang and J. Burgdörfer, Phys. Rev. A **49**, 2470 (1994). doi:10.1103/PhysRevA.49.2470.

[50] G.S. Ezra, K. Richter, G. Tanner and D. Wintgen, J. Phys. B: At. Mol. Opt. Phys. **24**, L413 (1991). doi:10.1088/0953-4075/24/17/001.

[51] K. Richter and D. Wintgen, Phys. Rev. Lett. **65**, 1965–1965 (1990). doi:10.1103/PhysRevLett.65.1965.

[52] K. Richter and D. Wintgen, J. Phys. B: At. Mol. Opt. Phys. **24**, L565 (1991). doi:10.1088/0953-4075/24/23/002.

[53] K. Richter, J.S. Briggs, D. Wintgen and E.A. Solov'ev, J. Phys. B: At. Mol. Opt. Phys. **25**, 3929 (1992). doi:10.1088/0953-4075/25/19/007.

[54] R.P. Madden and K. Codling, Phys. Rev. Lett. **10**, 516–518 (1963). doi:10.1103/PhysRevLett.10.516.

[55] J.Z. Tang and I. Shimamura, Phys. Rev. A **50**, 1321 (1994). doi:10.1103/PhysRevA.50.1321.

[56] A. Menzel, S.P. Frigo, S.B. Whitfield, C.D. Caldwell and M.O. Krause, Phys. Rev. A **54**, 2080 (1996). doi:10.1103/PhysRevA.54.2080.

[57] R.R. Freeman and D. Kleppner, Phys. Rev. A **14**, 1614–1619 (1976). doi:10.1103/PhysRevA.14.1614.

[58] R.R. Jones and T.F. Gallagher, Phys. Rev. A **38**, 2846–2853 (1988). doi:10.1103/PhysRevA.38.2846.

[59] F. Roussel, M. Cheret, L. Chen, T. Bolzinger, G. Spiess, J. Hare and M. Gross, Phys. Rev. Lett. **65**, 3112 (1990). doi:10.1103/PhysRevLett.65.3112.

[60] L. Pruvost, P. Camus, J.M. Lecomte, C.R. Mahon and P. Pillet, J. Phys. B: At. Mol. Opt. Phys. **24**, 4723 (1991). doi:10.1088/0953-4075/24/22/011.

[61] J. Boulmer, P. Camus and P. Pillet, J. Opt. Soc. Am. B **4**, 805 (1987). doi:10.1364/JOSAB.4.000805.

[62] P. Camus, C.R. Mahon and L. Pruvost, J. Phys. B: At. Mol. Opt. Phys. **26**, 221 (1993). doi:10.1088/0953-4075/26/2/006.

[63] J.G. Story, L.D. Van Woerkom and W.E. Cooke, J. Opt. Soc. Am. B **4** (5), 811 (1987). doi:10.1364/JOSAB.4.000811.

[64] S. Cohen, P. Camus and A. Bolovinos, J. Phys. B: At. Mol. Opt. Phys. **38**, S1–S16 (2005). doi:10.1088/0953-4075/38/2/001.

[65] U. Eichmann, V. Lange and W. Sandner, Phys. Rev. Lett. **68**, 21 (1992). doi:10.1103/PhysRevLett.68.21.

[66] K.D. Heber, M. Seng, M. Halka, U. Eichmann and W. Sandner, Phys. Rev. A **56**, 1255 (1997). doi:10.1103/PhysRevA.56.1255.

[67] R.P. Wood and C.H. Greene, Phys. Rev. A **49**, 1029 (1994). doi:10.1103/PhysRevA.49.1029.

[68] J.E. Hansen, C. Laughlin, H.W. van der Hart and G. Verbockhaven, J. Phys. B: At. Mol. Opt. Phys. **32**, 2099 (1999). doi:10.1088/0953-4075/32/9/305.

[69] E. Luc-Koenig, A. Lyras, J.M. Lecomte and M. Aymar, J. Phys. B: At. Mol. Opt. Phys. **30**, 5213 (1997). doi:10.1088/0953-4075/30/22/018.

[70] E. Luc-Koenig, M. Aymar, J.M. Lecomte and A. Lyras, J. Phys. B: At. Mol. Opt. Phys. **31**, 727 (1998). doi:10.1088/0953-4075/31/4/020.

[71] J.M. Lecomte, M. Telmini, M. Aymar and E. Luc-Koenig, J. Phys. B: At. Mol. Opt. Phys. **27**, 667 (1994). doi:10.1088/0953-4075/27/4/008.

[72] C.H. Greene and C. Jungen, in *Advances in Atomic and Molecular Physics*, edited by D.R. Bates and B. Bederson, Vol. 21 (Academic Press, Orlando, 1985), pp. 51–121.

[73] C. Jungen, *Molecular Applications of Quantum Defect Theory* (Taylor & Francis, New York, London, 1996).

[74] G. Miecznik and C.H. Greene, J. Opt. Soc. Am. B **13**, 244 (1996). doi:10.1364/JOSAB.13.000244.

[75] P.G. Burke, *R-Matrix Theory of Atomic Collisions*, *Springer Series on Atomic, Optical, and Plasma Physics*, Vol. 61 (Springer Berlin Heidelberg, Berlin, Heidelberg, 2011).

[76] G. Wang, J. Wan and X. Zhou, J. Phys. B: At. Mol. Opt. Phys. **43**, 035001 (2010). doi:10.1088/0953-4075/43/3/035001.

[77] W.C. Chu, H.L. Zhou, A. Hibbert and S.T. Manson, J. Phys. B: At. Mol. Opt. Phys. **42**, 205003 (2009). doi:10.1088/0953-4075/42/20/205003.

[78] S.A. Bhatti, C.L. Cromer and W.E. Cooke, Phys. Rev. A **24**, 161 (1981). doi:10.1103/PhysRevA.24.161.

[79] C.L. Pekeris, Phys. Rev. **115**, 1216 (1959). doi:10.1103/PhysRev.115.1216.

[80] Y. Accad, C.L. Pekeris and B. Schiff, Phys. Rev. A **4**, 516–536 (1971). doi:10.1103/PhysRevA.4.516.

[81] E.A. Hylleraas, Z. Phys. **54** (5-6), 347 (1929). doi:10.1007/BF01375457.

[82] G.W.F. Drake, Phys. Rev. Lett. **65**, 2769 (1990). doi:10.1103/PhysRevLett.65.2769.

[83] S.P. Goldman, Phys. Rev. Lett. **73**, 2547 (1994). doi:10.1103/PhysRevLett.73.2547.

[84] G. Lagmago Kamta, B. Piraux and A. Scrinzi, Phys. Rev. A **63**, 040502 (2001). doi:10.1103/PhysRevA.63.040502.

[85] D.P. Carroll, H.J. Silverstone and R.M. Metzger, J. Chem. Phys. **71** (10), 4142 (1979). doi:10.1063/1.438187.

[86] Y. Ho, Phys. Rep. **99**, 1 (1983). doi:10.1016/0370-1573(83)90112-6.

[87] W.P. Reinhardt, Annu. Rev. Phys. Chem. **33**, 223 (1982). doi:10.1146/annurev.pc.33.100182.001255.

[88] B.R. Junker, in *Advances in Atomic and Molecular Physics*, edited by D.R. Bates and B. Bederson, Vol. 18 (Academic Press, New York, 1982), pp. 207–263.

[89] J. Aguilar and J.M. Combes, Commun. Math. Phys. **22**, 269–279 (1971). doi:10.1007/BF01877510.

[90] E. Balslev and J.M. Combes, Commun. Math. Phys. **22**, 280–294 (1971). doi:10.1007/BF01877511.

[91] B. Grémaud and P. Gaspard, J. Phys. B: At. Mol. Opt. Phys. **31** (8), 1671 (1998). doi:10.1088/0953-4075/31/8/017.

[92] P. Schlagheck and A. Buchleitner, Eur. Phys. J. D **22**, 401–415 (2003). doi:10.1140/epjd/e2003-00017-9.

[93] Y.K. Ho and J. Callaway, J. Phys. B: At. Mol. Phys. **18**, 3481 (1985). doi:10.1088/0022-3700/18/17/010.

[94] Y.K. Ho, Z. Phys. D. **11**, 277 (1989). doi:10.1007/BF01438499.

[95] K.T. Chung and B.F. Davis, Phys. Rev. A **26**, 3278 (1982). doi:10.1103/PhysRevA.26.3278.

[96] J. Eiglsperger, B. Piraux and J. Madroñero, Phys. Rev. A **80**, 022511 (2009). doi:10.1103/PhysRevA.80.022511.

[97] J. Eiglsperger, B. Piraux and J. Madroñero, Phys. Rev. A **81**, 042527 (2010). doi:10.1103/PhysRevA.81.042527.

[98] J. Eiglsperger, B. Piraux and J. Madroñero, Phys. Rev. A **81**, 042528 (2010). doi:10.1103/PhysRevA.81.042528.

[99] J. Eiglsperger, M. Schönwetter, B. Piraux and J. Madroñero, At. Data Nucl. Data Tables **98**, 120 (2012). doi:10.1016/j.adt.2011.11.003.

[100] A. Buchleitner, B. Grémaud and D. Delande, J. Phys. B: At. Mol. Opt. Phys. **27**, 2663 (1994). doi:10.1088/0953-4075/27/13/001.

[101] D. Wintgen and D. Delande, J. Phys. B: At. Mol. Opt. Phys. **26**, L399 (1993). doi:10.1088/0953-4075/26/14/004.

[102] B. Simon, Phys. Lett. A **71** (2-3), 211 (1979). doi:10.1016/0375-9601(79)90165-8.

[103] N. Moiseyev, Phys. Rep. **302**, 212 (1998). doi:10.1016/S0370-1573(98)00002-7.

[104] N. Moiseyev, *Non-Hermitian Quantum Mechanics* (Cambridge University Press, Cambridge, 2011).

[105] C.W. McCurdy, M. Baertschy and T.N. Rescigno, J. Phys. B: At. Mol. Opt. Phys. **37**, R137 (2004). doi:10.1088/0953-4075/37/17/R01.

[106] M. Baertschy, T.N. Rescigno, W.A. Isaacs, X. Li and C.W. McCurdy, Phys. Rev. A **63**, 022712 (2001). doi:10.1103/PhysRevA.63.022712.

[107] T.N. Rescigno, W.A. Isaacs, A.E. Orel, H.D. Meyer and C.W. McCurdy, Phys. Rev. A **65**, 032716 (2002). doi:10.1103/PhysRevA.65.032716.

[108] P.L. Bartlett, A.T. Stelbovics and I. Bray, J. Phys. B: At. Mol. Opt. Phys. **37**, L69 (2004). doi:10.1088/0953-4075/37/4/L01.
[109] F.L. Yip, T.N. Rescigno and C.W. McCurdy, Phys. Rev. A **94**, 063414 (2016). doi:10.1103/PhysRevA.94.063414.
[110] F. Morales, F. Martín, D.A. Horner, T.N. Rescigno and C.W. McCurdy, J. Phys. B: At. Mol. Opt. Phys. **42**, 134013 (2009). doi:10.1088/0953-4075/42/13/134013.
[111] N. Elander, S.B. Levin and E. Yarevsky, Int. J. Quantum Chem. **109** (3), 459 (2009). doi:10.1002/qua.21829.
[112] M. Génévriez, D. Wehrli and F. Merkt, J. Chem. Phys. **153** (7), 074311 (2020). doi:10.1063/5.0015608.
[113] D. Wehrli, M. Génévriez, S. Knecht, M. Reiher and F. Merkt, J. Chem. Phys. **153**, 074310 (2020). doi:10.1063/5.0015603.
[114] R. Čurík, D. Hvizdoš and C.H. Greene, Phys. Rev. Lett. **124**, 043401 (2020). doi:10.1103/PhysRevLett.124.043401.
[115] J. Royal and A.E. Orel, Phys. Rev. A **73**, 042706 (2006). doi:10.1103/PhysRevA.73.042706.
[116] V.P. Majety and A. Scrinzi, J. Phys. B: At. Mol. Opt. Phys. **48**, 245603 (2015). doi:10.1088/0953-4075/48/24/245603.
[117] T. Carette, J.M. Dahlström, L. Argenti and E. Lindroth, Phys. Rev. A **87**, 023420 (2013). doi:10.1103/PhysRevA.87.023420.
[118] D.A. Telnov, K.E. Sosnova, E. Rozenbaum and S.I. Chu, Phys. Rev. A **87**, 053406 (2013). doi:10.1103/PhysRevA.87.053406.
[119] M. Génévriez, D. Wehrli and F. Merkt, Phys. Rev. A **100**, 032517 (2019). doi:10.1103/PhysRevA.100.032517.
[120] D.A. Telnov and S.I. Chu, Phys. Rev. A **59**, 2864 (1999). doi:10.1103/PhysRevA.59.2864.
[121] A. Mihelič, Phys. Rev. A **98**, 023409 (2018). doi:10.1103/PhysRevA.98.023409.
[122] D. Wehrli, M. Génévriez and F. Merkt, Phys. Rev. A **100**, 012515 (2019). doi:10.1103/PhysRevA.100.012515.
[123] G. Fields, X. Zhang, F.B. Dunning, S. Yoshida and J. Burgdörfer, Phys. Rev. A **97**, 013429 (2018). doi:10.1103/PhysRevA.97.013429.
[124] R.D. Cowan, *The Theory of Atomic Structure and Spectra*, *Los Alamos Series in Basic and Applied Sciences* (University of California Press, Berkeley, 1981).
[125] E. Persson, S. Yoshida, X.M. Tong, C.O. Reinhold and J. Burgdörfer, Phys. Rev. A **68**, 063406 (2003). doi:10.1103/PhysRevA.68.063406.
[126] T.N. Rescigno and C.W. McCurdy, Phys. Rev. A **62**, 032706 (2000). doi:10.1103/PhysRevA.62.032706.
[127] D. Manolopoulos and R. Wyatt, Chem. Phys. Lett. **152**, 23–32 (1988). doi:10.1016/0009-2614(88)87322-6.
[128] C.W. McCurdy, D.A. Horner, T.N. Rescigno and F. Martín, Phys. Rev. A **69**, 032707 (2004). doi:10.1103/PhysRevA.69.032707.
[129] C.W. McCurdy and F. Martín, J. Phys. B: At. Mol. Opt. Phys. **37** (4), 917 (2004). doi:10.1088/0953-4075/37/4/017.
[130] H. Bachau, E. Cormier, P. Decleva, J.E. Hansen and F. Martín, Rep. Prog. Phys. **64**, 1815 (2001). doi:10.1088/0034-4885/64/12/205.
[131] N. Elander and E. Yarevsky, Phys. Rev. A **57**, 3119 (1998). doi:10.1103/PhysRevA.57.3119.
[132] N. Rom, E. Engdahl and N. Moiseyev, J. Chem. Phys. **93**, 3413 (1990). doi:10.1063/1.458821.
[133] G. Yao and S.I. Chu, Chem. Phys. Lett. **204** (3-4), 381 (1993). doi:10.1016/0009-2614(93)90025-V.
[134] J. Wang, S.I. Chu and C. Laughlin, Phys. Rev. A **50**, 3208–3215 (1994). doi:10.1103/PhysRevA.50.3208.
[135] C. Lanczos, J. Res. Natl. Bur. Stan. **45**, 255 (1950). doi:10.6028/jres.045.026.
[136] K. Wu and H. Simon, SIAM J. Matrix Anal. Appl. **22**, 602–616 (2000). doi:10.1137/S0895479898334605.
[137] T.F. Gallagher, J. Opt. Soc. Am. B **4**, 794 (1987). doi:10.1364/JOSAB.4.000794.
[138] A. Kramida, Y. Ralchenko, and J. Reader, NIST atomic spectra database (Ver. 5.7.1) (National Institute of Standards and Technology, 2019). doi:10.18434/T4W30F
[139] S.P. Goldman, Phys. Rev. Lett. **78**, 2325 (1997). doi:10.1103/PhysRevLett.78.2325.
[140] Ch. Jungen and S.C. Ross, Phys. Rev. A **55**, R2503 (1997). doi:10.1103/PhysRevA.55.R2503.